Quantitative Brain SPECT in Alzheimer's Disease and Normal Aging

Keith A. Johnson, Marie F. Kijewski, J. Alex Becker, Basem Garada, Andrew Satlin and B. Leonard Holman

Departments of Medicine (Neurology Division) and Radiology, Brigham and Women's Hospital; and Harvard Medical School, Boston, Massachusetts; Departments of Neurology and Psychiatry and Magnetic Resonance Imaging Center, McLean Hospital, Belmont, Massachusetts; and the Department of Physics, Massachusetts Institute of Technology, Cambridge, Massachusetts

To improve the diagnostic utility of brain single-photon emission computed tomography (SPECT) in Alzheimer's disease (AD), we have developed and evaluated an objective method of differentiating patients and healthy elderly controls using a quantitative image analysis protocol. HMPAO-SPECT image datasets from 29 patients with probable AD and 78 age-matched controls were registered to a common anatomic frame of reference. Activity levels within 120 standardized cortical volumes were determined by an automated procedure. Subjects were classified into normal and AD groups by quadratic discriminant analysis using two features: global average activity level and average normalized activity levels within the two clusters of standardized volumes identified as most significantly different in AD by analysis of covariance. The classification used split-half replication to ensure valid results. Classification performance quantified by the area under a binormal ROC curve fitted to the data was 0.923 ± 0.036; at a threshold likelihood ratio of 1, the sample sensitivity was 91% and specificity was 86%. We conclude that quantitative SPECT accurately distinguishes AD patients from elderly controls.

J Nucl Med 1993; 34:2044–2048

Studies demonstrating abnormal regional cerebral perfusion or metabolism in patients with Alzheimer's disease (AD) (*1–8*) have led to investigation of the accuracy of functional images in the diagnosis of AD. Image analysis methods have relied on visual interpretation of radiotracer activity patterns or statistical analysis of activity ratios within subjectively specified regions of interest (ROI). An objective method of extracting information from functional brain image datasets would more fully exploit the available quantitative information and may lead to a more accurate diagnosis of AD. We have developed a perfusion brain SPECT image analysis method and tested it in a group of AD patients and normal control subjects.

Received Mar. 11, 1993; revision accepted July 19, 1993.

For correspondence and reprints contact: Keith A. Johnson, MD, Dept. of Radiology, Brigham and Women's Hospital, Boston, MA 02115.

METHODS

Patients and Control Subjects

Patients (n = 29) were referred from the McLean Hospital Memory Diagnostic Center and the Massachusetts General Hospital Memory Disorders Unit. Each patient met research criteria of the National Institute for Neurological Diseases and Stroke/Alzheimer's Disease and Related Disorders Association (NINDS-ADRDA) for the diagnosis of "probable Alzheimer's disease" (*9*). There were 11 males and 18 females (mean age (±s.d.) was 73.0 ± 7.9 yr; range, 55–84, Table 1). Patients were examined by a neurologist, underwent CT and/or MR imaging, and had routine hematologic and serum chemistry studies. The diagnosis of probable AD was made without knowledge of SPECT results. Dementia severity was assessed with a structured mental status examination, the Blessed Dementia Scale (BDS) (*10*). The BDS is composed of two subtests: one that assesses personality change and performance of activities of daily living, and a second that measures memory, orientation and concentration. A score of 0 to 2 is normal, and a score of 67 indicates maximal dementia severity. Patients' BDS scores ranged from 3 to 56 (mean ± s.d., 24.7 ± 15.6).

Control subjects (n = 78) were referred from the Massachusetts Institute of Technology Clinical Research Center where each was extensively examined medically and neurologically as part of an ongoing study of normal aging. Each subject had normal physical and neurological examinations, and normal tests of serum chemistry, hematology and liver and thyroid functions. In addition, each underwent a standardized battery of neuropsychologic tests to document any impairments in specific cognitive domains. Subjects were extensively screened in this way to eliminate those with signs of early cognitive impairment. There were 40 males and 28 females; mean age (±s.d.) was 69.6 ± 8.3 yr (range 55–92 yr), which did not significantly differ from AD patients (t-test $p > 0.06$) (Table 1).

SPECT Acquisition

SPECT images were acquired using a dedicated brain imaging instrument (ASPECT, Digital Scintigraphics, Inc., Waltham, MA) equipped with a stationary annular NaI crystal and a rotating collimator system (*12*). The measured system resolution in air using capillary line sources was 8.2 mm at the center and 7.3 mm at 9 cm from the center for ^{99m}Tc (*12*). Images were acquired 20 min after intravenous injection of 20.0 mCi (±1.0 mCi) of ^{99m}Tc-HMPAO (Ceretec, Amersham Ltd., Amersham, UK), with patients supine, at rest, with eyes open, in a darkened room. Total acquisition time was 20 or 30 min. Two pulse-height analyzer

TABLE 1
Demographic Data for Alzheimer's Disease Patients and Normal Control Subjects

	Age (yr)	Sex (M:F)	BDS†
AD	73.0 ± 7.9*	11:18	24.7±
15.6			
(n = 29)	(55–84)		(3–56)
Controls	69.6 ± 8.3‡	40:38	n.a.
(n = 78)	(55–92)		

*Values are mean ± s.d. (range); n.a. indicates not applicable.
†Blessed Dementia Scale.
‡Mean age not significantly different from AD group by Student's t-test ($p > 0.06$).

windows were employed with one set at 140 ± 14 keV and one set to acquire scatter information at 119 ± 7 keV. These two datasets were stored as separate arrays controlled by an array processor.

After acquisition was complete, collimator/crystal normalizations were performed on each dataset. The scatter correction method (*13*), which is standard on the ASPECT, was applied. The projections were prefiltered using a Butterworth filter (cutoff = 0.175 cycles per pixel; power factor = 10). Sixty-four slices were reconstructed in a 128 × 128 matrix with each pixel measuring 1.67 × 1.67 mm, and attenuation corrected (*14*).

Quantitative Analysis

Data were obtained using a supervised, automated procedure that yielded ^{99m}Tc-HMPAO activity levels (mean counts per voxel) in cortical regions. This procedure comprised three steps.

Standard Orientation. Each three-dimensional dataset was displayed simultaneously in transaxial, sagittal and coronal planes and each plane was rotated to conform to a standard orientation, defined as follows: maximal right-left symmetry of petrous bone activity voids defined the transaxial plane by rotating the dataset about y; the frontal and occipital poles defined the sagittal plane by rotations about x; and maximal symmetry of the caudate heads defined the coronal plane by rotations about z. This procedure minimized differences in anatomic orientation between subjects. The reoriented three-dimensional datasets were transferred to a DECstation 5000/200 (Digital Equipment Corp., Maynard, MA) for further processing.

Transaxial Reference Slice Selection. To standardize the range of slices along the z-axis to be averaged and analyzed, we identified the 1.67-mm slice which contained the most superior portion of the thalami. This served as the "seed" slice. To identify the seed slice, uniform scaling of gray-scale values was applied to the entire 64-slice dataset. The topmost transaxial slice in which activity from the thalami was at 90% or greater of the maximum activity in the whole brain was defined as the seed slice.

Identification of "Macrovoxels". The seed slice was averaged with the two slices above and the two slices below to provide meanslice 0. Two adjacent meanslices were calculated from above and two from below meanslice 0, yielding five meanslices, each with a thickness of 1.67 mm × 5 = 8.35 mm, which is approximately equal to the FWHM resolution of the ASPECT system.

Contours delineating the brain surface in meanslices −2, −1, 0, 1 and 2 were generated by a semi-automated edge detection algorithm implemented on the DECstation (*15*). An ellipse approximating the brain surface in slice −2 was used as a guide by the algorithm as it interactively generated a detailed contour based on pixel intensity and its derivative. A contour consisted of a set of points $\{(r_i, \theta_i), i = 0, N - 1\}$ where N is the number of points in the contour, r_i is the distance of point i from the center of the guiding ellipse, and $\theta_i = 2\pi(i/N)$ is the polar angle of the point i measured counterclockwise relative to the horizontal line passing through the center of the ellipse. Individual surface contouring accomplished cross-sectional (i.e., x-y plane) scaling, compensating for differences in brain size between subjects. Contours in the four higher slices were automatically generated using the parameters and contours of previous slices. Contours were edited as necessary to define the brain surface in cases where background activity was relatively high.

The contour in each slice was then used to define the outer margin of a circumferential region centered over cortical activity in each slice. The circumferential region for each slice was defined to be the image area bounded by the contours $\{(r_i, \theta_i), i = 0, N - 1\}$ and $\{(0.8r_i, \theta_i), i = 0, N - 1\}$. This area was divided into 24 parts ("macrovoxels"), such that macrovoxel n consisted of image pixels in the portion of the circumferential region defined by $2\pi(n/24) \leq \theta < 2\pi((n + 1)/24)$, where n = 0, 23. Thus, the inner margin of the region was concentric with the outer contour and located closer to the center by a factor of 0.8 along any radius. A total of 120 macrovoxels (24 × 5 averaged slices) were identified in each SPECT dataset.

Statistical Analyses. We used analysis of covariance (ANCOVA) (*16*) to assess the significance of changes in patterns of regional activity between disease and control groups, controlling for variation in counts in a reference volume. This technique is designed to eliminate "global" effects which cause between-subjects differences in brain tracer uptake. It was proposed by Friston et al. (*17*) and applied to PET data on a voxel-by-voxel basis. The analysis is based on the model:

$$Y = \beta_0 + \beta_1 X + \beta_2 Z + \beta_3 XZ + \text{error}. \qquad \text{Eq. 1}$$

For our application, the dependent variable Y is the mean activity within a particular macrovoxel and the independent variable X is the mean activity within the reference volume. For this study of AD patients, the reference volume consisted of the two posterior macrovoxels in the four lowest slices which fall within the medial occipital lobe. Z is a dummy variable which takes the values 0 and 1 for the two subject groups. Valid application of ANCOVA requires that β_3 is 0, i.e., the group data can be represented by parallel regression lines. Parallelism was established for each macrovoxel by a large-sample z-test of a hypothesis that the regression coefficients for lines fitted separately to the data for each group are different (*16*). Given that the assumption of parallelism is valid, the data can be fitted to the reduced model:

$$Y = \beta_0 + \beta_1 X + \beta_2 Z + \text{error}. \qquad \text{Eq. 2}$$

The change in regional activity that can be attributed to disease is represented by β_2, i.e., the vertical distance between the regression lines for the normal and AD groups. The null hypothesis that β_2 equals zero was tested for each macrovoxel using a partial F test (*16*). The ANCOVA yielded a group of macrovoxels that differed significantly between the two groups (see Results). This information guided selection of the features used in a discriminant analysis, and revealed for each macrovoxel the relationship between macrovoxel activity and average occipital activity for use in normalization.

Discriminant analysis (*18*) is a method of classifying individuals

into groups based on the values of features derived from the images. We used three features: mean cortical activity (within the 120 macrovoxels) and regional activity, normalized to occipital activity using ANCOVA slopes, within two clusters of macrovoxels identified by ANCOVA as most significantly different between the normal and AD groups. The macrovoxel activity values A_{ij} were normalized for subject occipital activity level O_j by $\hat{A}_{i,j} = A_{i,j} + \beta_i (O_s - O_j)$, where O_s is an arbitrary standard occipital activity level and β_i is the slope of the regression lines fitted by ANCOVA for macrovoxel i. Quadratic rather than linear analysis was used because data for the two groups could not be characterized by a common covariance matrix ($p < 0.001$). For each subject, the analysis yielded a likelihood ratio that the subject belonged to the AD rather than the normal group. Binormal ROC curves were fitted (*19*) to data generated by varying the criterion for assignment to the AD rather than the normal group, i.e., by calculating true-positive and false-positive rates for a number of threshold likelihood ratios. Classification performance of the method was quantified by the area under the curve (*20*). To avoid bias introduced by resubstitution, i.e., testing a classification method by classifying the same subjects used to establish the method, we used a crossvalidation (split-half replication) procedure whereby each half of the subjects was classified on the basis of mean vectors and covariance matrices calculated from the other half.

RESULTS

Normalized ^{99m}Tc-HMPAO uptake was significantly reduced (ANCOVA; $p < 0.001$) in AD patients compared to normal control subjects in 43/112 macrovoxels (Fig. 1). Significantly reduced HMPAO uptake was found in left (18 macrovoxels) and right (15 macrovoxels) temporoparietal, and left (4 macrovoxels) and right (6 macrovoxels) frontal regions. These results were not corrected for multiple comparisons, however, <1 significant macrovoxel would be expected by chance at $p = 0.001$. Moreover, the clustering of significantly different macrovoxels makes it even more unlikely that the results are due to chance. Because each macrovoxel is composed of a large number of image voxels (~500), spatial correlation in noise between adjacent macrovoxels is negligible (*21,22*). Because of the much greater than expected number of highly significantly different macrovoxels and the clustering, we conclude that these macrovoxels represent locations of change in brain perfusion due to AD.

The parallelism assumption required for ANCOVA was rejected at the $p = 0.001$ level for only three macrovoxels. At the $p = 0.01$ level, the assumption was rejected for 20 macrovoxels, however, only two of these were among those found significantly different at the $p = 0.001$ level. From these results we conclude that the ANCOVA model is appropriate for quantifying changes in brain activity patterns due to AD.

The quadratic discriminant analysis used three features: global average activity and average normalized activity within two clusters of macrovoxels identified by ANCOVA. The two clusters corresponded to the contiguous groups (11 left and 5 right parietal) of macrovoxels that were the most significantly different (Fig. 1, dark blue regions). The likelihood ratios (of belonging to the AD rather than the normal group) for individual subjects are plotted in Figure 2. A likelihood ratio of 1 implies equal probability of belonging to either group. The sample sensitivity for these data (using resubstitution) was 94% and specificity was 86% (Fig. 2). The area under the binormal ROC curve fitted to data generated by the discriminant analysis using the more robust crossvalidation technique was 0.923 ± 0.036. At a threshold likelihood ratio of 1, the sample sensitivity was 91% and specificity was 86% which is expected for new patients being imaged in our clinic.

DISCUSSION

Quantitative methods for evaluating functional neuroimaging in the aged population are essential because changes in the normally aging brain overlap those seen in neurodegenerative disease. We developed a quantitative method in which radiolabeled tracer activity in cortical regions was sampled from a standardized brain volume. Our method represents a departure from ROI-based methods and has the following features: (1) Global effects were controlled with an ANCOVA normalization procedure, adapted from Friston et al. (*17*), which permitted the isolation of regional group differences. (2) A large number of voxels was examined in each brain, without the use of anatomically specified, operator-dependent ROI placement. (3) The ANCOVA resulted in selection of a cluster of macrovoxels which were used in a discriminant analysis to classify each case into AD or normal groups. We validated this procedure using split-half replication, and evaluated performance using ROC techniques (*20*). (4) Our method compensated for differences in underlying brain volume between normals and AD patients by measuring activity in volumes defined by surface contours. Artifactually reduced perfusion due to brain atrophy was therefore less likely to be a factor in diagnostic accuracy. We recognize, however, that structural/functional image superposition and volume correction would be necessary to fully evaluate this issue. Our method successfully distinguished elderly normal subjects from patients with the clinical diagnosis of probable AD; 25 of 29 (86%) AD patients and 71 of 78 (91%) normal control subjects were correctly classified.

The accuracy of SPECT or PET in AD has been reported (*7,23–25*) in studies comparing visual image patterns or ROI measurements with clinical diagnosis established by strictly applying NIH criteria for "probable AD" (*9*). Accuracy of the NIH criteria evaluated at autopsy is reported to be approximately 80%–85% (*26*), but this level of accuracy was obtained in patients who were carefully screened in a research setting, followed over time, and required to be clinically uncomplicated (*24,27,28*). In the early stages of illness, patients may not yet satisfy these criteria and the diagnostic error rate has been estimated to be 30% (*29*).

The reported accuracy of functional imaging for AD defined by NIH criteria has varied widely and depended on

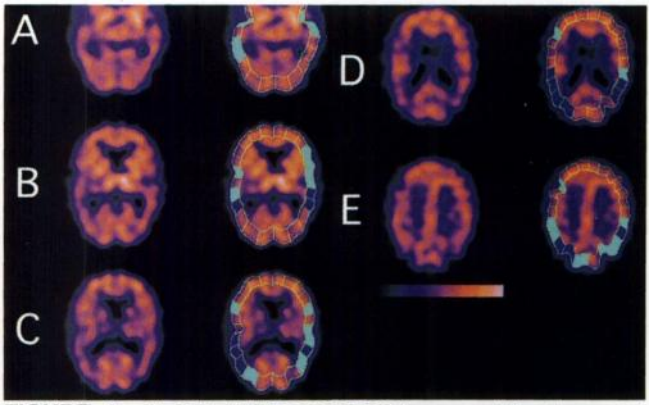

FIGURE 1. At right, HMPAO SPECT images at five transaxial levels from a patient with AD. At left, regions used in the discriminant functions (dark blue) and regions with significantly reduced perfusion ($p < 0.001$, dark blue or green) are shown superimposed on images from the same patient as at right.

the methods used for image classification. For example, Powers et al. (*24*), calculated sensitivity of 38% among 13 patients and specificity of 88% among 26 nonAD controls using only the presence of bilateral parietal perfusion defects seen with PET perfusion images. When abnormality in any brain region was used as the criterion, sensitivity was improved to 92% and specificity to 85%. Similar results have been obtained with SPECT (*7,23,30,31*), also using image pattern or ROI methods. Because of the wide variation in accuracy estimates, we sought to improve image analysis methods by minimizing subjectivity in pattern recognition or in the choice of ROI selected for measurement and by reducing the confounding effect of atrophy. Our method involved the use of discriminant functions which were calculated using both global activity and regional activity. Using PET perfusion images and an ROI-based method, Kippenhan et al. evaluated neural network and discriminant function classifiers in AD, and reported ROC areas of 0.85 and 0.80, respectively (*32*). The performance of our method, ROC area = 0.923 ± 0.036, exceeds that reported by Kippenhan et al., perhaps because we used a large number of standardized volumes acquired with higher spatial resolution, while they reduced their data to averages across large regions.

Functional neuroimaging is a potentially powerful clinical tool for evaluating the presence, extent and course of dementia, as well as response to putative therapies. The anatomic distribution of perfusion defects is characteristic of underlying symptomatology (*33,36*) and the severity of image abnormality parallels the severity of cognitive impairments (*4,6,7,35,36*). While our method successfully separated AD patients from control subjects, we cannot exclude the possibility that the features responsible for discriminating power were features of dementia, and not specifically of AD. The development of this type of method sets the stage for further studies of the heterogeneity of AD (*36,37*), as well as coexisting conditions such as parkinsonism and cerebrovascular disease.

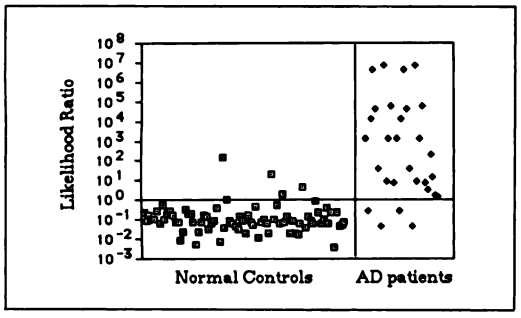

FIGURE 2. Plot of likelihood ratios resulting from the discriminant analysis for normal control subjects and patients with AD (25 of 29 (86%) AD patients and 73 of 78 (94%) normal control subjects were correctly classified).

REFERENCES

1. Frackowiak RSJ, Pozzilli C, et al. Regional cerebral oxygen supply and utilization in dementia. A clinical and physiological study with oxygen-15 and positron emission tomography. *Brain* 1981;104:753–778.
2. Friedland RP, Budinger TF, et al. Regional cerebral metabolic alterations in dementia of the Alzheimer type: positron emission tomography with (^{18}F)fluorodeoxyglucose. *J Comput Assist Tomogr* 1983;7:590–598.
3. Johnson KA, Mueller ST, et al. Cerebral perfusion imaging in Alzheimer's disease: use of single photon emission computed tomography and iofetamine hydrochloride ^{123}I. *Arch Neurol* 1987;44:165–168.
4. Jagust WJ, Budinger TF, Reed BR. The diagnosis of dementia with single photon emission computed tomography. *Arch Neurol* 1987;44:258–262.
5. Jagust WJ, Reed BR, et al. Alzheimer's disease. Age at onset and single-photon emission computed tomographic patterns of regional cerebral blood flow. *Arch Neurol* 1990;47:628–633.
6. Johnson KA, Holman BL, et al. Single photon emission computed tomography in Alzheimer's disease: abnormal iofetamine ^{123}I uptake reflects dementia severity. *Arch Neurol* 1988;45:392–396.
7. Johnson KA, Holman BL, et al. Iofetamine ^{123}I single photon emission computed tomography is accurate in the diagnosis of Alzheimer's disease. *Arch Intern Med* 1990;150:752–756.
8. Holman BL, Johnson KA, et al. The scintigraphic appearance of Alzheimer's disease: a prospective study using technetium-99m-HMPAO SPECT. *J Nucl Med* 1992;33:181–185.
9. McKhann G, Drachman D, et al. Clinical diagnosis of Alzheimer's disease: report of the NINCDS-ADRDA work group under the auspices of the Department of Health and Human Services Task Force on Alzheimer's Disease. *Neurology* 1984;34:939–944.
10. Blessed G, Tomlinson BE, Roth MN. The association between quantitative measures of dementia and of senile change in the cerebral grey matter of elderly subjects. *Br J Psychiatry* 1968;114:797–811.
11. Holman BL, Carvalho PA, et al. Brain perfusion SPECT using an annular single crystal camera: initial clinical experience. *J Nucl Med* 1990;31:1456–1461.
12. Genna S, Smith AP. The development of ASPECT, an annular single crystal brain camera for high efficiency SPECT. *IEEE Trans Nucl Sci* 1988;35:654–658.
13. Genna S, Pang SC, Burrows A. Analysis of an arcuate gamma camera design for transaxial reconstruction. *Medical Radionuclide Imag.*
14. Chang L-T. A method for attenuation correction in radionuclide computed tomography. *IEEE Trans Nucl Sci* 1978;25:638–643.
15. Becker JA, Johnson KA, et al. A unified processing environment for image fusion [Abstract]. *J Nucl Med* 1993;34:179.
16. Kleinbaum DG, Kupper LL. *Applied regression analysis and other multivariable methods.* North Scituate, MA: Duxbury Press; 1978.
17. Friston KJ, Frith CD, et al. The relationship between global and local changes in PET scans. *J Cereb Blood Flow Meas* 1990;10:458–466.
18. Wilf HS. *A method of coalitions in statistical discriminant analysis.* New York: Wiley; 1977.
19. Dorfman DD, Alf E. Maximum-likelihood estimation of parameters of signal-detection theory and determination of confidence intervals-rating-method data. *J Math Psychol* 1969;6:487–496.
20. Metz CE. ROC methodology in radiologic imaging. *Invest Radiol* 1986; 720–733.
21. Kijewski MF, Judy PF. The noise power spectrum of CT images. *Phys Med Biol* 1987;32:565–575.

22. Moore SC, Kijewski MF, et al. SPECT image noise power: effects of nonstationary projection noise and attenuation compensation. *J Nucl Med* 1988;29:1704–1709.
23. Eberling JL, Jagust WJ, et al. Reduced temporal lobe blood flow in Alzheimer's disease. *Neurobiol Aging* 1992;13:483–491.
24. Powers WJ, Perlmutter JS, et al. Blinded clinical evaluation of positron emission tomography for diagnosis of probable Alzheimer's disease. *Neurology* 1992;42:765–770.
25. Smith GS, deLeon MJ, et al. Topography of cross-sectional and longitudinal glucose metabolic deficits in Alzheimer's disease. *Arch Neurol* 1992;49: 1142–1150.
26. Joachim CL, Morris JH, et al. Clinically diagnosed Alzheimer's disease: autopsy results in 150 cases. *Ann Neurol* 1988;24:50–56.
27. Berg L, Hughes CP, et al. Mild senile dementia of Alzheimer type: research diagnostic criteria, recruitment and description of a study population. *J Neurol Neurosurg Psych* 1982;45:962–968.
28. Morris JC, McKeel DW Jr., Fulling K, et al. Validation of clinical diagnostic criteria for Alzheimer's disease. *Ann Neurol* 1988;24:17–22.
29. Khachaturian ZS. Diagnosis of Alzheimer's disease. *Arch Neurol* 1985;42: 1097–1105.
30. Reed BR, Jagust WJ, et al. Memory and regional cerebral blood flow in mildly symptomatic Alzheimer's disease. *Neurology* 1989;39:1537–1539.
31. Testa HJ, Snowden JS, et al. The use of ^{99m}Tc-HMPAO in the diagnosis of primary degenerative dementia. *J Cereb Blood Flow Metab* 1988;8:S123–S126.
32. Kippenhan JS, Barker WW, et al. Evaluation of a neural-network classifier for PET scans of normal and Alzheimer's disease subjects. *J Nucl Med* 1992;33:1459–1467.
33. Haxby JV, Duara R, et al. Relations between neuropsychological and cerebral metabolic asymmetries in early Alzheimer's disease. *J Cereb Blood Flow Metab* 1985;5:193–200.
34. Haxby JV, Grady CL, et al. Neocortical metabolic abnormalities precede nonmemory cognitive defects in early Alzheimer's disease-type dementia. *Arch Neurol* 1986;43:882–885.
35. de Leon M, Ferris SH, et al. Computed tomography and positron transaxial tomography evaluations of normal aging and Alzheimer's disease. *J Cereb Blood Flow Metab* 1983;3:391–394.
36. Haxby JV, Grady CL, et al. Heterogeneous anterior-posterior metabolic patterns in dementia of the Alzheimer type. *Neurology* 1988;38:1853–1864.
37. Chui HC, Teng EL, et al. Clinical subtypes of dementia of the Alzheimer type. *Neurology* 1985;35:1544–1550.